Thermal Imaging

35.1 Essential Components
35.2 Thermal Imaging Wavebands
35.3 Emission from Source
35.4 Atmospheric Transmission
35.5 Detectors
Photon Detectors • Thermal Detectors • Detector Performance Measures • Detector Cooling
35.6 Electronics
35.7 Optics and Scanning
35.8 Temperature References
35.9 Imager Performance
SNR and NETD • Minimum Resolvable Temperature Difference
35.10 Available Imagers
35.11 Performance Trade-offs
35.12 Future Trends in Thermal Imaging

Herbert M. Runciman
Pilkington Optronics

All objects at temperatures above absolute zero emit electromagnetic radiation. Radiation thermometry makes use of this fact to estimate the temperatures of objects by measuring the radiated energy from selected regions. Thermal imaging takes the process one stage further and uses the emitted radiation to generate a picture of the object and its surroundings, usually on a TV display or computer monitor, in such a way that the desired temperature information is easily interpreted by the user.

Thermal imagers require no form of illumination to operate, and the military significance of this, together with their ability to penetrate most forms of smoke, has been largely responsible for driving thermal imager development. Although thermal imagers intended for military or security applications can be used for temperature measurement, they are not optimized for this purpose since the aim is to detect, recognize, or identify targets at long ranges by their shape; thus, resolution and sensitivity are favored over radiometric accuracy.

35.1 Essential Components

All thermal imagers must have a detector or array of detectors sensitive to radiation in the required waveband, and optics to form an image of the object on the detector. In modern thermal imagers, the detector array might have a sufficient number of sensitive elements to cover the focal plane completely (a “staring array”), in the same way as a CCD television camera. Some of the most recent staring arrays can give good performance without cooling. In other imagers, the detector might take the form of a single row or column of elements, in which case a scanning mechanism is required to sweep the image across the detector array. If a single-element detector, or a very small detector array, is used, a means of

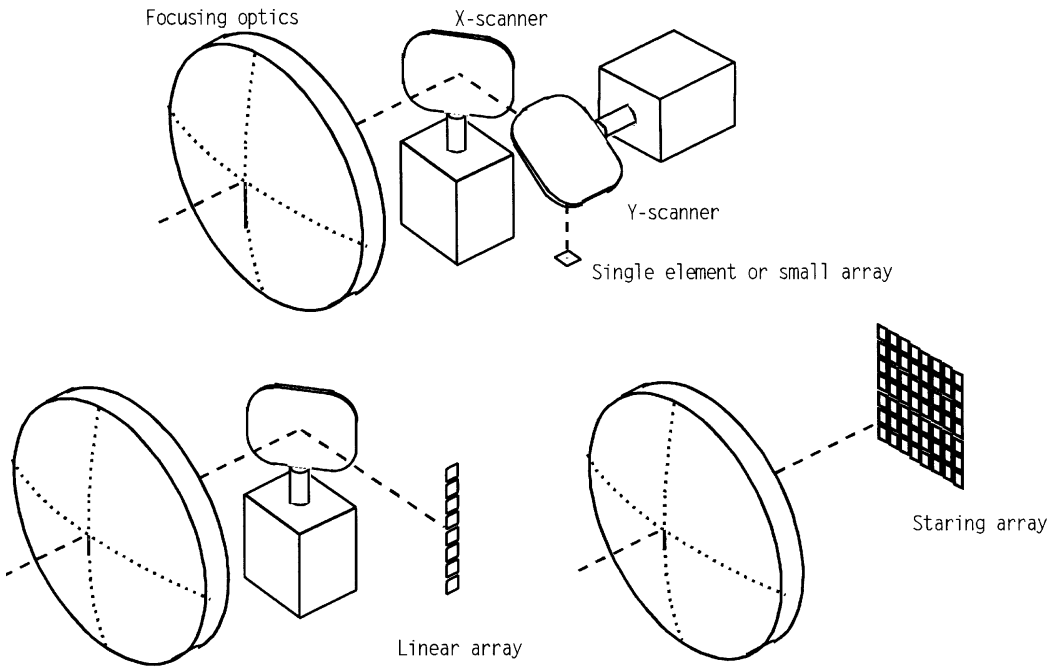

FIGURE 35.1 Thermal imaging options: (a) 2-D scanning for small detector array or single element; (b) 1-D scanning with linear detector array; (c) staring array without scanning.

providing a two-dimensional scan is required. (Figure 35.1 shows these options schematically.) For scanning imagers, it is necessary to cool the detectors (usually to about 80 K to 120 K) to achieve adequate performance.

Although in principle it would be possible to deduce target temperature from the absolute value of the detector signal, it is necessary in practice to estimate temperature by comparison with one or more reference bodies of known temperature. The temperature references are usually internal to the equipment, and accessed by mechanical movement of the reference (which may take the form of a rotating chopper) or by deflecting the optical path using a mirror.

35.2 Thermal Imaging Wavebands

The optimum waveband for thermal imaging is determined partly by the wavelength distribution of the emitted radiation, partly by the transmission of the atmosphere, and partly by the chosen detector technology.

The power radiated from a given area of an object depends only on its temperature and the nature of its surface. If the surface absorbs radiation of all wavelengths completely, it is referred to as a "blackbody." It then also emits the maximum amount possible, which can be calculated using the Planck equation (given later). Figure 35.2(a) shows the way in which blackbody emission varies with wavelength for several temperatures. It will be seen that for objects near normal ambient temperature, maximum output occurs at a wavelength of about 10 μm, or about 20 times the wavelength of visible light. At wavelengths below about 3 μm, there is generally insufficient energy emitted to allow thermal imaging of room-temperature objects. The emissivity at any wavelength is defined as the ratio of the energy emitted at that wavelength to the energy that would be emitted by a blackbody at the same wavelength.

It is important that the atmosphere should have sufficient transparency to permit the target to be observed. There are two important "atmospheric windows" — one between 3 μm and 5 μm (with a notch at 4.2 μm due to carbon dioxide absorption) and one between 7.5 μm and 14 μm. These are commonly

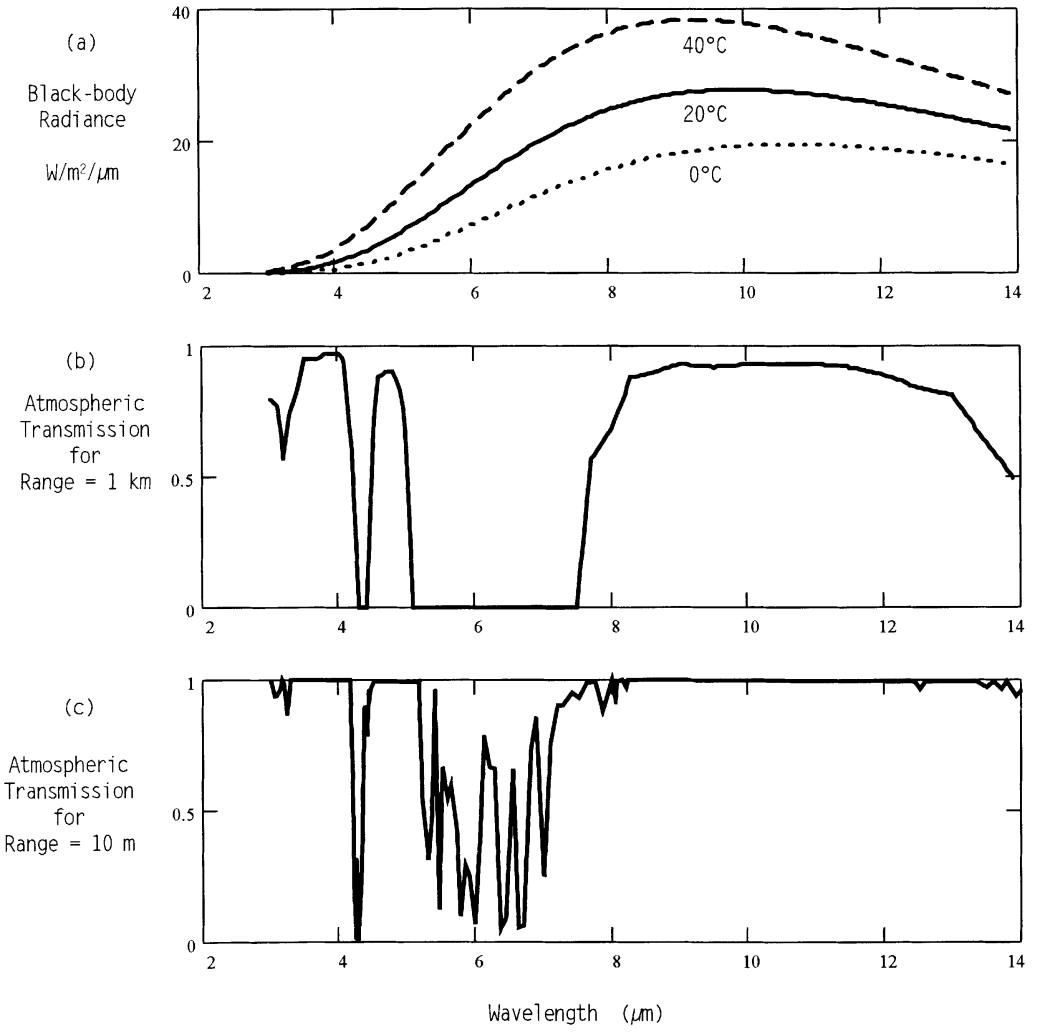

FIGURE 35.2 Factors determining thermal imaging wavebands. Imager must operate in regions where radiance is sufficiently high (a) and atmospheric transmission is good (b) and (c).

referred to as the medium-wave infrared (MWIR) and long-wave infrared (LWIR) windows, respectively. For thermal measurement over short ranges in the laboratory, it is possible to work outside these bands, but most instruments are optimized for either the MWIR or LWIR. Typical transmissions through 1 km and 10 m of a clear U.S. Standard Atmosphere are shown in Figures 35.2(b) and 35.2(c).

Emissivity for most naturally occurring objects and organic paints is high (>0.8) in the LWIR, but is lower and more variable in the MWIR. Metallic surfaces have low emissivity in both bands. Solar radiation in the MWIR is significant, and can cause errors in measurements made outdoors. These considerations favor the LWIR for quantitative imaging, but the band chosen can also be influenced by the chosen detector technology, the latter frequently being determined by cost. Scanning imagers can be used in either band, but are more sensitive for a given detector architecture in the LWIR. Cooled staring arrays give similar sensitivity in either band, but are currently more readily available in the MWIR. Uncooled staring arrays work well only in the LWIR band.

For temperature measurement, the electronics can be used to encode signal level as false color, a color scale derived from the thermal references being injected into the display to allow the user to identify the temperature of the object under examination. For general surveillance, a conventional gray-scale image

is usually preferred. Imagers for thermography can also include emissivity compensation. If accurate results are required for an object of low emissivity, it is important to ensure that the temperature of anything that might be reflected by the object is known and that the emissivity is accurately known. If the object is accessible, another object placed beside it with the same surface characteristics but known temperature can be used for calibration.

35.3 Emission from Source

The spectral radiance $W(\lambda,T)$ of a blackbody at temperature T and wavelength λ is given by the Planck equation [1]. For temperature differences between the target and the reference of a few degrees, it is frequently sufficiently accurate to assume a linear dependence of radiance on temperature difference, making the temperature derivative of the blackbody equation, $dW(\lambda,T)/dT$, more relevant. In the case of photon detectors, the detector output is proportional to the photon flux, which can be derived from the radiance using the fact that photon energy $E(\lambda) = hc/\lambda$, where h is the Planck constant. The total photon flux $N(\lambda)$ and its derivative with respect to temperature are thus relevant in this case. The equations are as follows:

$$W\left(\lambda,T\right)=\frac{c_1}{\lambda^5\left(e^{\frac{c_2}{\lambda T}}-1\right)},\quad \text{W m}^{-2}\ \mu^{-1} \tag{35.1}$$

$$N\left(\lambda,T\right)=\frac{c_3}{\lambda^4\left(e^{\frac{c_2}{\lambda T}}-1\right)},\quad \text{photons s}^{-1}\ \text{m}^{-2}\ \mu\text{m}^{-1} \tag{35.2}$$

$$\frac{dW\left(\lambda,T\right)}{dT}=\frac{c_1c_2e^{\frac{c_2}{\lambda T}}}{\lambda^6T^2\left(e^{\frac{c_2}{\lambda T}}-1\right)},\quad \text{W m}^{-2}\ \mu\text{m}^{-1}\ \text{K}^{-1} \tag{35.3}$$

$$\frac{dN\left(\lambda,T\right)}{dT}=\frac{c_3c_2e^{\frac{c_2}{\lambda T}}}{\lambda^5T^2\left(e^{\frac{c_2}{\lambda T}}-1\right)},\quad \text{photons s}^{-1}\ \text{m}^{-2}\ \mu\text{m}^{-1}\ \text{K}^{-1} \tag{35.4}$$

where: Numerical values of the constants are:

$c_1 = 3.742 \times 10^8$

$c_2 = 1.439 \times 10^4$

$c_3 = 1.884 \times 10^{27}$

The unit of wavelength is chosen for convenience to be the micrometer (μm).

The above values are for radiation into a hemisphere. The intensities (watts per steradian, photons per steradian, etc.) are obtained by dividing the above values by π. The actual radiances for real targets are obtained by multiplying by the spectral emissivity $\varepsilon(\lambda)$; but since target reflectivity $\rho(\lambda) = 1 - \varepsilon(\lambda)$, some caution is required. For example, a target at temperature T surrounded by a background of temperature T_b will appear to emit $W(\lambda,T)\varepsilon(\lambda) + W(\lambda,T_b)\rho(\lambda) = [W(\lambda,T) - W(\lambda,T_b)]\varepsilon(\lambda) + W(\lambda,T_b)$.

Provided that the background surrounds the target and that the target is reasonably small, the background acts as an isothermal enclosure, which can be shown [2] to behave as an ideal blackbody (i.e., $\varepsilon(\lambda) = 1$). The differential spectral radiance against background $\Delta W(\lambda)$ is thus $[W(\lambda,T) - W(\lambda,T_b)]\varepsilon(\lambda)$, which for a small temperature difference ΔT is simply:

$$\Delta W\left(\lambda\right) = \varepsilon\left(\lambda\right)\frac{\mathrm{d}W\left(\lambda,T\right)}{\mathrm{d}T}\Delta T \tag{35.5}$$

The spectral emissivity of a wide variety of natural and man-made objects is also given in [2].

A major difference between thermal imaging and visual imaging is the very low contrast. In the MWIR, the contrast calculated from Equation 35.1 due to 1 K at the target is about 4%, falling to about 2% in the LWIR.

35.4 Atmospheric Transmission

Provided that the absorption bands shown in Figures 35.2(b) and 35.2(c) are avoided, atmospheric transmission can frequently be ignored in the laboratory or industrial context. For longer ranges, an atmospheric transmission model must be used or calibrating sources must be placed at the target range. The standard atmospheric transmission model is LOWTRAN [3], currently at version 7. The atmospheric transmission $T_a(\lambda)$ reduces the differential signal from the target proportionately, but has no effect on the background flux if the atmosphere is at background temperature. Atmospheric transmission in the LWIR is severely affected by high humidity, making the MWIR the band of choice for long-range operation in the Tropics. (Many gases and vapors such as methane or ammonia have very strong absorptions in the infrared, making thermal imaging a possible means of leak detection and location.)

35.5 Detectors

There are two main types of detector — photon (or quantum) and thermal. A more detailed discussion of photon detectors is given in this handbook in Chapter 8.1.1 and 8.1.2, and of thermal detectors in Chapter 6.1.8, so only aspects unique to thermal imaging are discussed here.

Photon Detectors

In photon detectors, the response is caused by photons of radiation that generate free carriers in a semiconductor, which in turn increase the conductivity (for photoconductive detectors) or generate a potential difference across a junction (for photovoltaic detectors). Photovoltaic devices have the advantage of not requiring a bias current (important to reduce the heat load on the cooling system), and they have 40% lower noise because the electric field at the junction separates the carriers, thereby eliminating recombination noise. Whether or not the lower noise is achieved in practice depends on the read-out electronics. The photon energy in the LWIR is only about $1/20^{th}$ of that of a photon in the visible region of the spectrum, so a semiconductor with a much smaller bandgap than silicon must be used. The most widely used material is a compound of mercury, cadmium, and tellurium (MCT or CMT) since not only is the quantum efficiency excellent (70% or more), but the bandgap can be tuned to the desired wavelength (in either waveband) by altering the composition. Cooling of the detector to about 80 K is desirable for the LWIR, but about 120 K is acceptable for the MWIR. For the MWIR, indium antimonide (InSb) is also an excellent material; and since it is a true stoichiometric compound, it is easier to achieve good uniformity of response, but cooling to 80 K is required.

Detectors for use in scanning systems are frequently arranged so that several elements are scanned over the same part of the scene in rapid succession, the output of each element being delayed and added

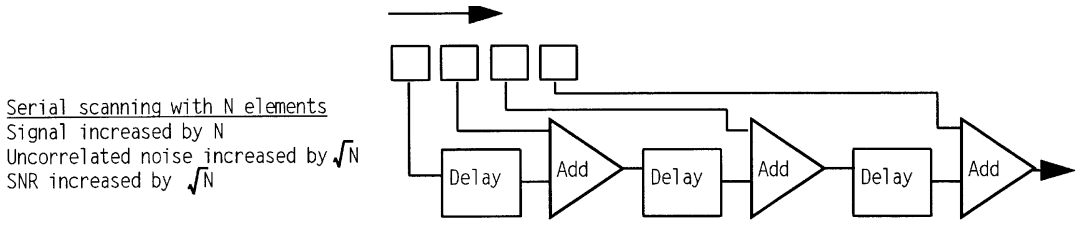

FIGURE 35.3 Use of serial scanning to enhance signal-to-noise ratio. The delay times are chosen to match the speed at which the image is swept along the detector array. Serial scanning is usually combined with parallel scanning using a detector matrix.

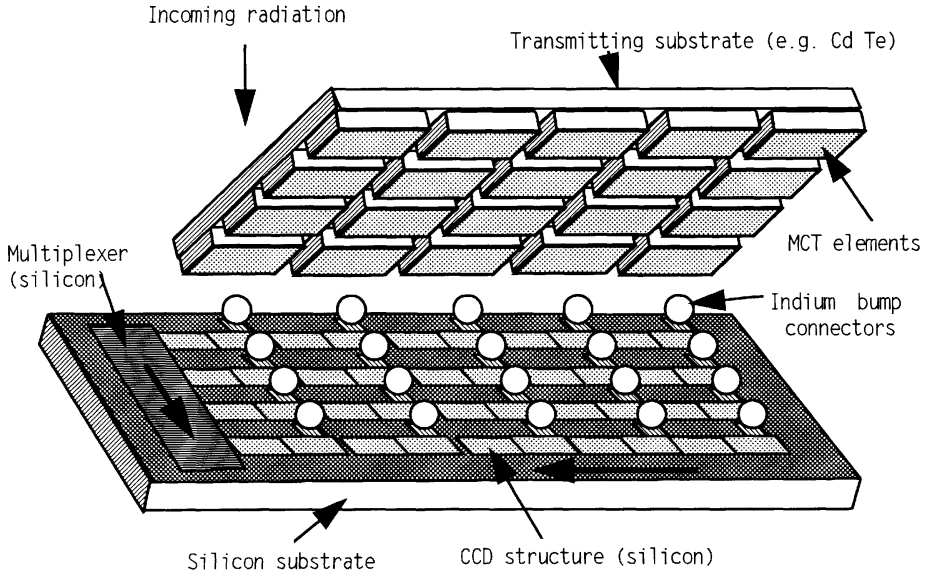

FIGURE 35.4 Typical hybrid detector construction. A typical element size is 30 μm. A large array of this type to match U.S. TV standard would have 640 × 480 elements.

to the previous one to enhance the signal-to-noise ratio (SNR). This approach (Figure 35.3) is termed serial scanning or "time-delay and integrate" (TDI) mode, and gives a theoretical gain in the SNR equal to the square root of the number of elements in TDI. It is also possible to perform TDI in the detector material itself. In the SPRITE detector (Signal Processing In The Element), the sensitive element is an elongated strip of CMT. Photons incident on the device generate carriers that drift toward a read-out electrode near one end. If the image is scanned along the detector at the same speed as the carrier drift, the signal builds up along the length of the device. The useful length is limited by carrier recombination, while diffusion of the carriers limits spatial resolution.

Large arrays of photon detectors are generally of hybrid construction, the sensitive elements being bonded to a silicon CCD or CMOS addressing circuit using indium "bumps" (Figure 35.4). An exception is the Schottky barrier detector (e.g., platinum silicide), which can be manufactured by a monolithic process, and thus tends to be lower in cost, but quantum efficiency is much lower and operation is usually limited to the MWIR band. Detector arrays and read-out architectures are discussed in depth in [2] Vol. 3, p. 246-341 and [4].

The detector assembly is encapsulated in a Dewar as shown in Figure 35.5. In front of the detector is a "cold shield" that limits the acceptance angle of the radiation to match that of the optics.

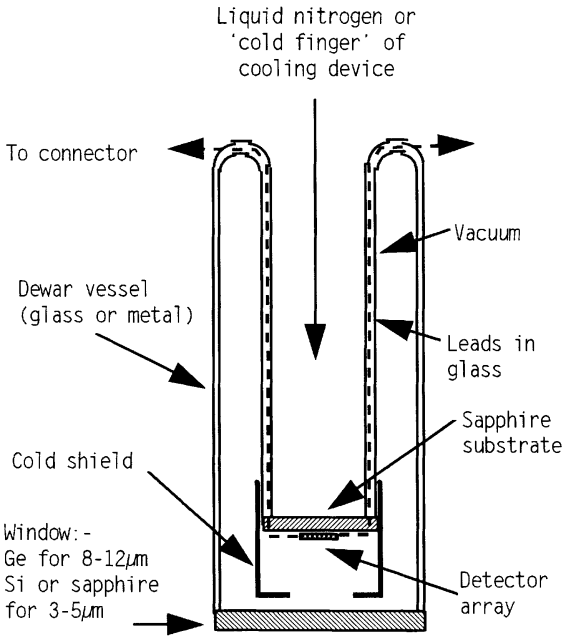

FIGURE 35.5 Construction of typical cooled detector. Cooling can be by liquid nitrogen, Joule-Thomson expansion of compressed gas, or a cooling engine.

Thermal Detectors

Thermal detectors rely on the heating effect of the incoming radiation, the change in temperature causing a change in resistance, capacitance, or electrical polarization that might be detected electrically. They are generally fairly slow in response (several milliseconds) but have the advantage that cooling is not essential (although it can be of considerable benefit with some types). The detectivity of uncooled thermal detectors is typically 1/100 that of cooled photon detectors, so real-time imaging requires the use of staring arrays. The essentials of a pyroelectric array are shown in Figure 35.6. Incoming radiation is absorbed by the blackened electrode, and the heat generated is transferred to the pyroelectric layer, which comprises a dielectric material that has been polarized by means of a high electric field during manufacture. The change in electrical polarization with temperature gives the electric signal. One of the most important parameters is the thermal isolation of the sensitive elements, so some kind of insulating support structure is necessary; and for good performance, the device must be evacuated to prevent convection. In a variant of this approach, the dielectric bolometer, the rapid variation of the dielectric constant at temperatures near the Curie point, causes the capacitance of the sensitive element to change, and hence the voltage for a constant charge. A detailed description of this approach is given in [5]. In both techniques, the detector responds only to change in temperature, so it is necessary to modulate the incoming radiation using a chopper. In the technique used initially by Wood [6] (now licensed to several manufacturers), the sensitive elements are vanadium dioxide coatings that undergo a large change in resistivity for a small temperature change. The elements are supported by silicon strips that are micromachined from the substrate and give excellent thermal insulation of the element. Changes in resistivity are read out by circuitry on the substrate, and no chopping is required, but the array must be maintained at a precise and uniform temperature.

Detector Performance Measures

The wavelength-dependent power responsivity of a detector $R(\lambda)$ is defined as the output potential or current that would result from 1 W of radiation at wavelength λ, assuming that linearity was maintained at such a high flux level. The units are V W^{-1} or A W^{-1}. Photon responsivities in V photon^{-1} s^{-1} and A photon^{-1} s^{-1} are similarly defined.

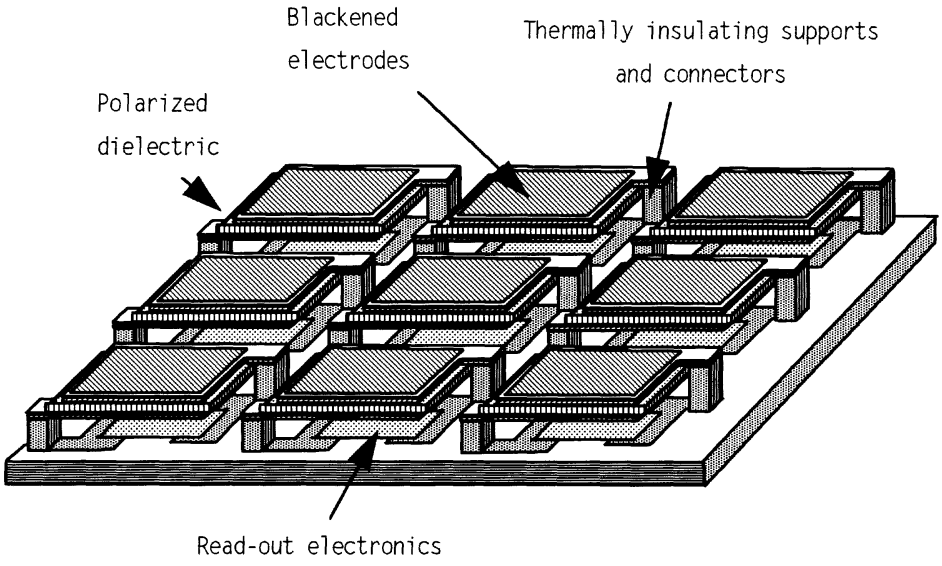

FIGURE 35.6 Essentials of an uncooled thermal detector array. The device is shown as pyroelectric or dielectric bolometer, but the essentials for a resistive bolometer are similar if the capacitors are replaced by resistors.

A thermal detector has a power responsivity that is essentially independent of wavelength, the limits of response being determined by the transparency of the window and the absorption spectrum of the element or the material used to blacken it.

In an ideal photon detector, the quantum efficiency η (defined as the number of carriers generated per photon) would be constant at all wavelengths for which the photon energy is greater than the bandgap, i.e., the photon responsivity is independent of wavelength up to the chosen cut-off wavelength. Since a given number of Watts corresponds to a number of photons proportional to the wavelength, the power responsivity (V W^{-1} or A W^{-1}) would increase linearly with wavelength until the cut-off. In practice, the cut-off is spread over about 0.5 μm and shortwave performance is modified by window transmission and antireflection coatings.

The sensitivity of a detector is limited by noise that may be due to the detector itself or due to the background radiation (as is discussed later). Noise-equivalent power NEP(λ) is defined as the power incident on the detector at wavelength λ, which gives a signal equal to the rms noise when the measurement is made with a 1-Hz bandwidth. The NEP depends also on the modulation frequency, the latter effect being large for thermal detectors, but frequently negligible for quantum detectors. For many types of detector, the noise is proportional to the square root of the sensitive area A_d and the electrical bandwidth B, so that $\sqrt{(A_d B)}$/NEP is constant. A performance figure that is proportional to sensitivity can then be defined as specific detectivity $D^*(\lambda) = \sqrt{(A_d B)}/\mathrm{NEP}(\lambda)$. For historical reasons, specific detectivity is usually given in units of cm$\sqrt{\mathrm{Hz}}$ W^{-1}, so it is important to remember to convert this to SI units or to measure detector area in square centimeters. Since noise is an electrical quantity particular to the detector under the conditions for which D^* is defined and is independent of wavelength, NEP(λ) is proportional to $1/R(\lambda)$; so if the value of detectivity D^*_p at the wavelength of peak responsivity R_p is known, for other wavelengths $D^*(\lambda) = D^*_p(R(\lambda)/R_p)$. Sometimes, "blackbody $D^*(T)$" figures are quoted rather than D^*_p. If the blackbody temperature is T, the value of D^*_p is given by:

$$D_p^* = \frac{D^*(T)R_p \int_0^\infty W(\lambda,T)\mathrm{d}\lambda}{\int_0^\infty W(\lambda,T)\mathrm{R}(\lambda)\mathrm{d}\lambda} \tag{35.6}$$

The rms noise voltage V_n is simply the NEP multiplied by the responsivity. Since the ratio $D^*(\lambda)/R(\lambda)$ is independent of wavelength, one obtains:

$$V_n = \sqrt{A_d B}\,\frac{R_p}{D_p^*} \tag{35.7}$$

The detector also affects the modulation transfer function (MTF) of the imager, defined as the ratio of the modulation depth of the signal due to a target with sinusoidally varying brightness of spatial frequency f cycles per milliradian to the modulation depth from a similar target at very low frequency. If there are no limitations due to time constant, the MTF of a detector is due to its instantaneous field of view (IFOV), which is given by IFOV = x/F where F is the focal length of the optics. For example, a lens of 500-mm focal length used with a 50-μm square detector would give an IFOV of 0.1 mrad. Then,

$$\mathrm{MTF}_d = \frac{\sin\left(\pi \times f \times \mathrm{IFOV}\right)}{\pi \times f \times \mathrm{IFOV}} \tag{35.8}$$

For staring arrays, frequencies above 1/2 cycle per element pitch (the Nyquist frequency) give aliasing, and it is undesirable to rely on performance above this frequency.

Detector Cooling

The method with the lowest cost is to use liquid nitrogen poured directly into the detector Dewar, and many detector manufacturers supply detectors in Dewars with sufficient capacity for many hours of use per filling. Outside the laboratory, this technique is seldom practical, and a cooling engine (usually based on the Stirling thermodynamic cycle) is commonly used. The cost of such an engine has now fallen to a level where it no longer dominates the cost of the instrument, and power consumption is only a few watts to give cooling to 80 K. Dimensions vary widely, but a typical low-power cooling engine is about 40 mm × 40 mm × 60 mm excluding the length of the cold finger that lies inside the detector Dewar. A disadvantage is the relatively slow cool-down time (several minutes typically) and, where this is critical (as in military or security applications), Joule-Thomson cooling can be used. This method operates by expansion of air or nitrogen compressed to about 15 MPa through a nozzle, and can give cool-down times of a few seconds. Thermoelectric cooling (using the Peltier effect) can be used for temperatures down to about 200 K. Some detectors (e.g., lead selenide) have been designed to operate at this temperature in the 3 μm to 5 μm band, but thermoelectric cooling is inadequate for most types of photon detectors. A survey of cooling methods and devices is given in [2], Vol. 3, p. 345–431.

35.6 Electronics

The electronics architecture depends on the type of detector and the application, but typically electronics are required to provide bias and clocking signals to the detector, to amplify the low-level signals from the detector, to equalize the responses of the outputs from different detector elements, to provide scan conversion to a form suitable for display, and to provide image processing suitable to the application.

In scanning imagers with a small number of detector elements, the output of each detector element can be amplified continuously, the amplifier outputs then being multiplexed to give the required display. The bandwidth (important for estimating sensitivity) must be at least sufficient to accommodate the data rate, but too wide a bandwidth gives excess high-frequency noise. An approach frequently used for the measurement of sensitivity (e.g., [1], p. 167) is to make the electronics response equivalent to that of a single-pole filter with the 3-dB point placed at a frequency corresponding to 1/(2 × dwell time), in which case the bandwidth is:

$$B = \frac{\pi \times \mathrm{FOV_h} \times \mathrm{FOV_v} \times f_f}{4E \times N \times \mathrm{IFOV}^2} \tag{35.9}$$

where $\mathrm{FOV_h}$ and $\mathrm{FOV_v}$ = Horizontal and vertical fields of view, respectively
f_f = Field rate
E = Ratio of the active scan period to the total period
N = Number of parallel detector channels

Often high-frequency boost filters are used to compensate for optics and detector MTFs, in which case the noise bandwidth can be much increased. A commonly used criterion for the electronic filtering is to make the perceived noise independent of frequency up to the cut-off frequency of the detector.

To maintain good spatial resolution, it is desirable that the detector output be sampled at least twice during the dwell time so that the Nyquist frequency is not a major limitation [7]. Frequencies above the Nyquist frequency are changed by the sampling process into lower frequencies, a process known as aliasing. Thus, the fidelity of the image is affected so that noise that might be expected to be of sufficiently high frequency to be filtered out can appear within the passband. To avoid aliasing, a steep-cut filter is used to eliminate frequencies above the Nyquist frequency before sampling. In staring systems, the Nyquist sampling frequency is 1/2 cycle per element pitch, so a 256×256 element array would be limited to a resolution of 128 cycles per line. This can be overcome by using "microscan" (or μscan), in which the image is collected over a number of fields with an image shift performed optically between each field, the commonest patterns being diagonal (low implementation cost) and 2×2 with four fields per frame.

For large detector arrays, charge is usually accumulated on a capacitor associated with each pixel for an integration time τ (which can often be controlled independently of the frame rate or dwell time to prevent saturation), the capacitor being discharged when the pixel is read out. The effective bandwidth of such an integrator is:

$$B = \frac{1}{2\tau} \tag{35.10}$$

With state-of-the-art amplifiers, it is generally possible to make amplifier and read-out noise less than the detector noise, the exceptions being systems of small aperture that are "photon starved" and uncooled systems.

In multichannel systems, a crucial role of the electronics is to provide channel equalization. The importance of this is due to the very low contrast of the target against the background. If the full sensitivity of an imager with a typical NETD of 0.1 K is to be realized, the difference in response between adjacent detector channels must be less than 0.4% in the MWIR or 0.2% in the LWIR. In a real-time imager where the eye integrates over several frames, the requirement is 2 to 3 times more stringent, since nonuniformity, unlike signal-to-noise ratio, is not improved by eye integration.

35.7 Optics and Scanning

The materials commonly used for visual optics are opaque in the thermal wavebands. In the LWIR, germanium is by far the most widely used material. It has a refractive index of 4, and chromatic dispersion is sufficiently low that it is frequently unnecessary to use a second material for color correction. These properties allow high performance to be achieved with few optical components, largely offsetting the relatively high cost of the material. In the MWIR, germanium has fairly high dispersion, but silicon/germanium doublets give highly achromatic performance. Zinc selenide and zinc sulfide are commonly used for color correction, some forms of the latter being transparent also in the visible band. The high refractive indices make anti-reflection coating essential to reduce surface losses — the transmission of a thin piece

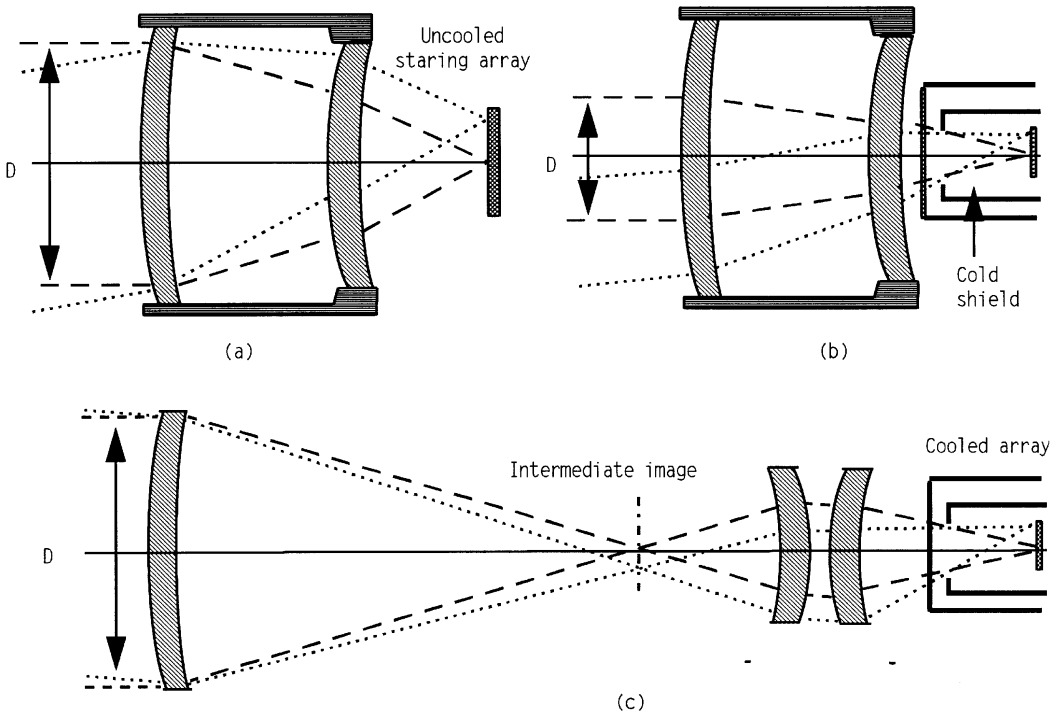

FIGURE 35.7 Optics for staring arrays. The same lens as is used for uncooled operation (a) can be used as in (b) for a cooled device, but re-imaging optics (c) are needed for a cooled imager to use the full aperture. In practice, the optics in (c) would usually have more components than shown.

of uncoated germanium is only 40%, rising to better than 99% when coated. Front-surface mirrors coated with aluminum or gold perform well in the thermal bands, and optics based on parabolic mirrors can be used if the detector array is small. For most applications, it is necessary to seal the imager to prevent ingress of dust or moisture, in which case a window is required, making reflecting optics less attractive than it first appears, since the cost of a mirror and window can be a little less than that of a lens. Plastic materials in general have poor transmission, although a thin polythene or "cling-wrap" window might be acceptable for laboratory use.

For uncooled staring arrays, the sole function of the optics is to focus an image of the scene on the detector. Good performance in the 8 μm to 12 μm band can be achieved with a two-element Petzval lens [8] with aspheric surfaces (Figure 35.7(a)). With a cooled array, it is desirable that the cold shield inside the detector should form the aperture stop of the system, since any radiation from the interior of the instrument will add to the system noise and might give shading effects. If the field of view is reasonably small, it is sometimes possible to use the same type of lens in the manner shown in Figure 35.7(b), but it can be seen that the beam diameter that can be accepted is now much smaller than the lens diameter; thus, for long-range applications requiring large beam diameters, the lens becomes very costly. The solution is to use re-imaging optics as shown in simplified form in Figure 35.7(c). The relay stage not only re-images the scene on the detector, but images the cold shield on the objective lens so that the latter need be no larger than the input beam. The intermediate image can be useful to allow insertion of temperature references or microscanning.

Scanning, when required, is most commonly performed by moving reflective surfaces since electro-optic and acousto-optic techniques either provide insufficient deflection angle or are highly wavelength dependent, causing smearing over the thermal wavebands. Rotating refractive polygons are now less used than previously. For fast line scanners, rotating reflective polygons (sometimes with curved facets) are

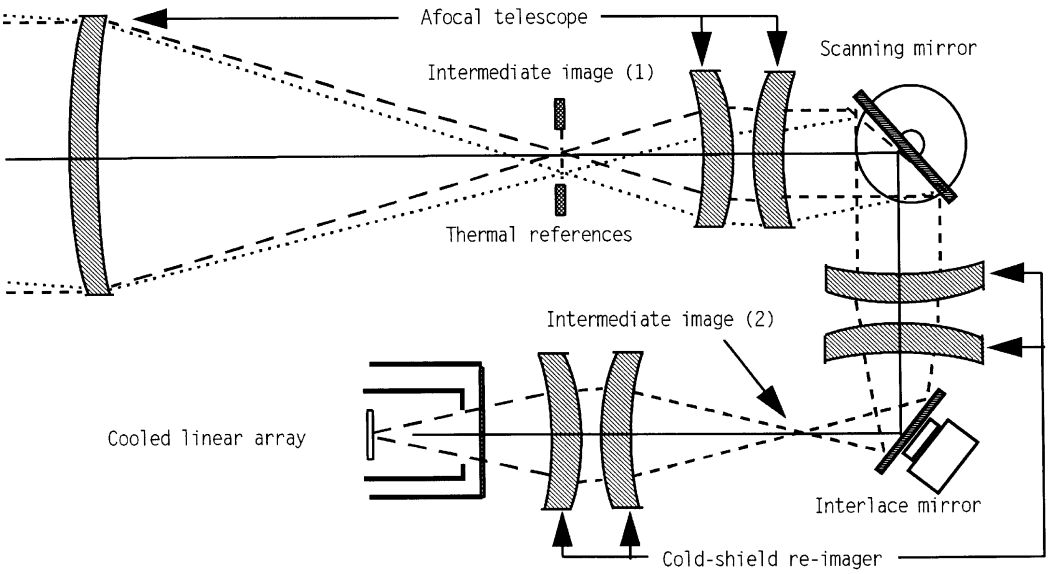

FIGURE 35.8 Optics for a linear array imager. The cold shield is imaged on the scanning mirror, and the scanning mirror is placed at the exit pupil of the telescope.

used, in some cases using gas-bearing motors operating in helium to reduce windage. For frame scanning, a plane mirror driven by a powerful galvanometer is customary. This can give very linear sweeps at 60 Hz with scan efficiencies of about 80% when operated in a closed loop. For microscan or interlace, a small image movement can be achieved by tilting a mirror using piezoelectric actuators or by tilting a refractive plate using a galvanometer. For scanning systems, it is generally necessary to re-image the detector cold shield at each scan mechanism, since otherwise the optics must be enlarged to accommodate pupil movements. Figure 35.8 shows how this is done in a typical imager using a linear array. The movement of the interlace mirror is sufficiently small that pupil re-imaging at this mirror is not required.

Figure 35.9 shows a typical arrangement for a 2-D scanner, a high-speed polygon rotor being used to generate the line scan.

The main optical parameters to be specified are transmission T_o, focal length F, and f/number $F_\#$ or numerical aperture (NA). Since IFOV = x/F, the focal length determines the spatial resolution for a given detector. The NA is defined as the sine of the semi-cone angle of the output beam from the optics. It can be shown that if a diffuse (Lambertian) source emits W W m^{-2} into a hemisphere, the radiance due to the source in the focal plane is $WT_o(\text{NA})^2$. $F_\#$ is defined as the ratio of focal length to diameter, and for a distant object NA = $1/(2F_\#)$, so the ratio of the irradiance in the focal plane to the source radiance is:

$$\frac{\text{Irradiance in focal plane}}{\text{Radiance from extended object}} = \frac{T_o(\lambda)T_a(\lambda)}{4F_\#^2} \tag{35.11}$$

Transmission of thermal imaging optics is typically 60% to 90%, depending on complexity. The transmission of any optics between the temperature reference and the target must be known for quantitative measurement.

The imaging performance of a lens can be indicated by the size of the spot generated in the focal plane by a distant point object, and accurate results can be obtained if the intensity as a function of the angle α from the center of the image (point spread function, PSF) is known. A more usual approach is to use

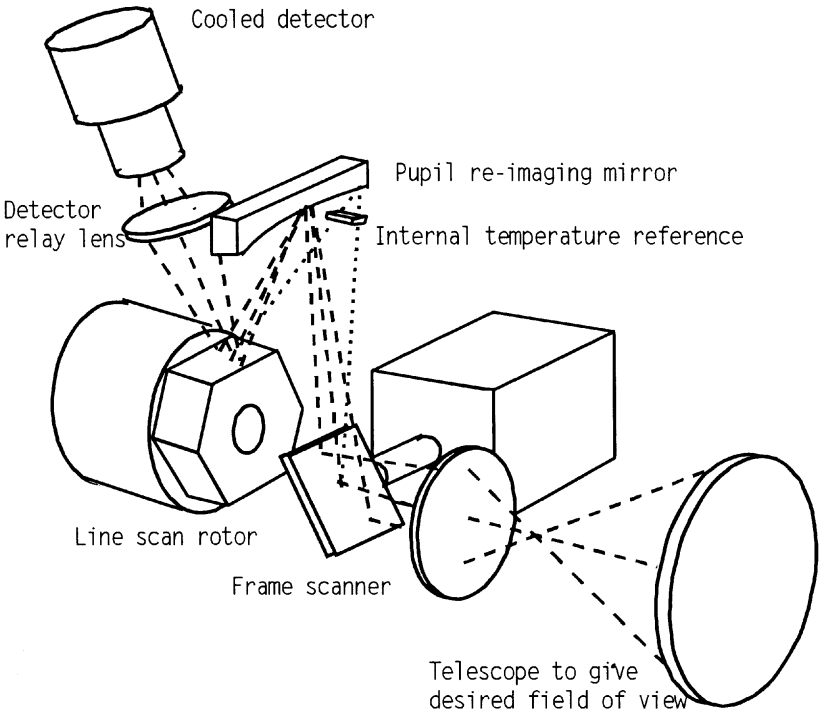

FIGURE 35.9 Simplified layout of imager using 2-D scanning (based on Pilkington Optronics HDTI). The line scan uses a high-speed polygon, and the concave strip mirror images the line scan pupil on the frame scanner.

the modulation transfer function (MTF), defined as the ratio of the contrast of the image of a target with a sinusoidal spatial variation in intensity to the contrast of the target itself. The MTF depends on the spatial frequency *f* of the target (expressed in cycles per radian) and on the wavelength of the radiation. For perfect optics of diameter *D*, diffraction gives the following values for PSF and MTF, which are also plotted in Figure 35.10:

$$\mathrm{PSF}(a) = 4\left[\left(\frac{\lambda}{\pi D a}\right) J_1\left(\frac{\pi D a}{\lambda}\right)\right]^2 \tag{35.12}$$

where J_1 is the Bessel function.

$$\mathrm{MTF}_o(f) = \frac{2}{\pi}\left\{\mathrm{a}\cos\left(\frac{\lambda f}{D}\right) - \frac{\lambda f}{D}\sqrt{1-\left(\frac{\lambda f}{D}\right)^2}\right\} \tag{35.13}$$

In practice, optics are frequently far from the diffraction limit, so manufacturers' figures must be used. If a thermal imager is to be used for measurement, correction for MTF will be required unless the IFOV and the PSF are both smaller than the region over which the temperature is to be measured. The signal level for a subresolution point source can be obtained by integrating the PSF over the detector area. For diffraction-limited optics, a rule of thumb for the LWIR band is that the diffraction spot diameter in mrad is the reciprocal of the lens diameter in inches (or 25/*D* when *D* is in millimeters).

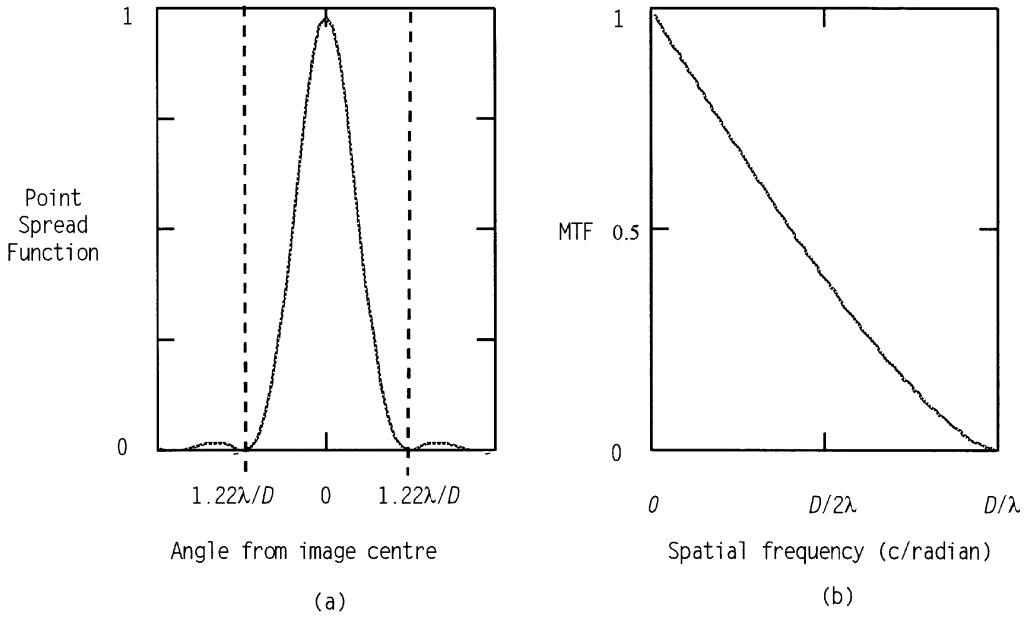

FIGURE 35.10 Point Spread Function (a) and MTF (b) for ideal optics of diameter D at wavelength λ. The first dark ring of the PSF has angular diameter $2.44\lambda/D$, and encircles 86% of the total energy. The MTF is zero for all frequencies above D/λ.

35.8 Temperature References

If a thermal imager is to be used for measurement, it is generally necessary to compare the signal from the target with that from one or more bodies at known temperature. The most precise results are obtained if two bodies at different known temperatures and having the same emissivity as the target (e.g., painted with the same paint type) are placed adjacent to the target and the target temperature is deduced by interpolation. There is then no dependence on emissivity, atmospheric transmission, and optical transmission. Outside the laboratory this is seldom practical, however, and it is necessary to use thermal references within the imager itself. The fewer optical components there are between the reference and the scene, the better will be the accuracy. If the interior of a cavity of uniform temperature is viewed through a small hole, the emission from the hole follows the Planck equation accurately, irrespective of the emissivity of the interior surface of the cavity. Although very accurate, such a blackbody cavity is usually inconveniently large, and it is more usual to use a blackened surface with deep grooves or pits to give high emissivity.

Unless the detector has only one element, thermal references are also desirable if not essential to allow the outputs of the different detector elements to be equalized.

35.9 Imager Performance

SNR and NETD

If the target is larger than the IFOV and the PSF, the signal level due to a small temperature difference is found by multiplying the source differential output, the atmospheric and optical transmissions, the geometric attenuation due to the *f*/number, the detector area, and the responsivity as derived or defined in the previous sections, and integrating over the imager passband to give:

$$V = \frac{A_d \Delta T}{4F_\#^2} \int R(\lambda) T_t(\lambda) T_a(\lambda) \varepsilon(\lambda) \frac{dW(\lambda, T)}{dT} d\lambda \tag{35.14}$$

The noise voltage V_n is given by Equation 35.7, so the signal-to-noise ratio is obtained. If the number of serial detector elements is N_s, the signal level is increased by this factor; but since the noise is uncorrelated between the elements, it increases only as $\sqrt{N_s}$, so SNR improves as $\sqrt{N_s}$. The SNR also improves as the square root of the number of parallel channels, since the dwell time is increased, giving a reduction in bandwidth B.

The sensitivity of a thermal imager for large targets is normally defined in terms of its noise equivalent temperature difference (NETD) — the temperature difference between a large blackbody at zero range and its background — which gives a signal equal to the rms noise. This is given by V_n/V when $\Delta T = 1$, $T_a = 1$ and $\varepsilon(\lambda) = 1$, and is found to be:

$$\text{NETD} = \frac{4F_\#^2}{\int_0^\infty D^*(\lambda) T_t(\lambda) \frac{dW(\lambda, T)}{dT} d\lambda} \sqrt{\frac{B}{A_d N_s}} \tag{35.15}$$

A good indication of signal-to-noise ratio is given if it is assumed that T_a and ε are constant within the imager passband, in which case SNR = $\varepsilon\, T_a\, \Delta T$/NETD.

Minimum Resolvable Temperature Difference

The performance of a thermal imager is frequently defined by its minimum resolvable temperature difference (MRTD). MRTD(f) is the temperature difference between a four-bar square test pattern of frequency f c mrad^{-1} and its background required for an observer to count the imaged bars. The test is subjective, but has the advantage of characterizing the complete system and display, including any effects of nonuniformity. MRTD is proportional to NETD, and inversely proportional to the MTF and the square root of the number of frames presented within the integration time of the eye τ_e. The constant of proportionality depends on the degree of overlap between the scan lines. Discussion of the full MRTD model is beyond the scope of this chapter, but a simple expression (based on [1] p.167) — which gives an indication of performance for an imager with square detector elements without overlap and at least two samples per IFOV, and in which the electronics bandwidth is the same as that used for NETD calculation — is:

$$\text{MRTD}(f) = \frac{3 \cdot \text{NETD} \cdot f \cdot \text{IFOV}}{\text{MTF}_o \text{MTF}_d \sqrt{\tau_e f_f}} \tag{35.16}$$

Calculation of MRTD is best performed using standard models, the most widely adopted being FLIR 92 [9] .

35.10 Available Imagers

Recent advances in detector technology are only now beginning to be incorporated in commercially available systems. The result is that product ranges are currently changing rapidly, and prices are very unstable. The prices for uncooled systems in particular are likely to drop significantly in the near future as the market size increases. An indication of cost at present is:

Military high-performance imagers $100,000–300,000
Medium-performance imagers for measurement $30,000–100,000
Uncooled imagers $10,000–30,000 (but falling rapidly)

TABLE 35.1 Typical Commercially Available Thermal Imagers

Manufacturer	Model	Data	Description
AGEMA	880 LWB	LWIR, CMT	Thermal measurement system
		NETD = 0.07	175 pixels (50% MTF)
Amber	Radiance1	MWIR, InSb	Compact imager for measurement
		NETD = 0.025	256 × 256 pixels, InSb
Amber	Sentinel	LWIR	Uncooled compact imager
		NETD = 0.07K	320 × 240 pixels
Cincinnati	IRRIS-160ST	MWIR, InSb	Compact imager
		NETD = 0.025	160 pixels/line
FLIR Systems	2000F	LWIR, CMT	Surveillance imager
		NETD = 0.1K	>350 pixels/line
GEC Sensors	Sentry	LWIR	Uncooled low-cost imager
			100 × 100 pixels
Hamamatsu	THEMOS 50	MWIR	Microscope, 4-μm resolution
		NETD = 0.2 K	256 × 256 pixels
Inframetrics	ThermaCAM	MWIR, PtSi	Thermal measurement system
		NETD<0.1K	256 × 256 pixels
Mitsubishi	IR-M600	MWIR, PtSi	High-definition imager
		NETD = 0.08K	512 × 512 pixels
Nikon	LAIRD-3	MWIR, PtSi	High-definition imager
		NETD = 0.1K	768 × 576 pixels
Pilkington Optronics	LITE	LWIR	Hand held surveillance imager
		NETD = 0.2K	350 × 175 pixels
Quest	TAM200	MWIR	Microscope with probe facility
		NETD = 0.05K	Bench system with 12.5-μm resolution

Prices reflect not only performance, but ruggedness, environmental survivability, and image processing software. Military imagers in many countries are based on "common modules" that are sometimes multisourced, and that must be configured for specific applications. Table 35.1 lists some typical commercial imagers, which were selected to emphasize the wide variety of imager types, and the list must not be taken as a comprehensive survey. Some compact imagers weigh less than 2 kg, while some of the bench systems weigh over 100 kg. Accuracy of temperature measurement is not generally specified, but ±2 K or ±2% is a good figure for a calibrated imager. The information is based on published brochures, and there is every likelihood that improved models will be available by the time this book is published. It is strongly recommended that prospective purchasers should contact as many manufacturers as possible to obtain specifications and prices.

35.11 Performance Trade-offs

The expression for NETD presented earlier is appropriate for evaluation of existing systems where D^* is known. To predict performance of future systems based on photon detectors, and to carry out design trade-offs, it is important to appreciate that D^* is very dependent on conditions of use and on waveband. One reason is that the photons from an object of given temperature, although having a well-defined average flux, are emitted at random times. Statistical theory shows that if on average N photons are collected within a given time interval, the standard deviation is $\sqrt{N}$ if N is large enough to make the distribution Gaussian (as is almost always the case in the infrared due to the high background flux). This "photon noise" frequently predominates, in which case the detector is referred to as BLIP (background-limited photodetector). The D^* is then determined more by the conditions of use than by the detector itself. If the efficiency of the cold shield η_c is defined as the ratio of the effective f/number for the background flux to that of the signal, the number of background electrons generated within an integration time τ is given by:

$$N_e = \frac{\tau A_d}{4F_\#^2 \eta_c^2} \int_0^\infty N(\lambda, T)\eta(\lambda)\mathrm{d}\lambda \tag{35.17}$$

For the reasons discussed above, the rms electron noise for a BLIP device within time τ is simply the square root of the above figure. If the detector also has read-out noise of N_n electrons rms, this could be regarded as the noise that would be caused by a background flux that caused the generation of N_n^2 photoelectrons, so the noise can be written as:

$$\text{Noise} = \sqrt{N_e + N_n^2} \text{ electrons rms} \tag{35.18}$$

The signal due to a temperature difference of 1 K between target and background expressed in electrons within the integration time is:

$$\text{Signal} = \frac{\tau A_d}{4F_\#^2} \int_0^\infty T_t(\lambda) T_a(\lambda) \eta(\lambda) \frac{\mathrm{d}N(\lambda, T)}{\mathrm{d}T} \mathrm{d}\lambda \tag{35.19}$$

Thus, the signal-to-noise ratio for ΔT = 1 K is found, NETD being simply 1/SNR when T_a = 1.

For staring systems, and some scanning systems, the integration time is limited by saturation. If the maximum number of electrons that can be stored is N_m, we find that the maximum integration time is:

$$\tau_m = \frac{4F_\#^2 \, \eta_c^2 \, N_m}{A_d \int_0^\infty N(\lambda)\eta(\lambda)\mathrm{d}\lambda} \tag{35.20}$$

When the integration time is controlled to restrict the number of electrons generated within the sampling interval to τ_m, the noise is given by letting $N_e = N_m$ in Equation 35.18, so is independent of *f*/number. If one also substitutes τ_m for τ in Equation 35.19, and divides Equation 35.19 by Equation 35.18, to obtain SNR, one obtains:

$$\text{SNR} = \frac{\Delta T \, \eta_c^2 \, N_m \int T_o(\lambda) T_a(\lambda) \eta(\lambda) \frac{\mathrm{d}N(\lambda, T)}{\mathrm{d}T} \mathrm{d}\lambda}{\sqrt{N_m + N_n^2} \int N(\lambda)\eta(\lambda)\mathrm{d}\lambda} \tag{35.21}$$

The ratio of integrals is effectively the contrast of the scene behind the optics, which is further reduced by the inefficiency of the cold shield; thus, performance depends mainly on image contrast at the detector and the number of electrons stored. (Quantum efficiency essentially cancels out; and for a saturated device, $\sqrt{N_m}$ is usually greater than N_n.)

The above formulae are sufficiently general to allow trade-offs for photon detectors to be carried out against aperture, waveband, range, and frame rate, the main uncertainty being the read-out noise. For staring array detectors with processing on the focal plane, a typical figure is N_n = 1000, but much better (and worse) values are possible. The SNR and NETD values obtained in this way are for a single pixel. If the samples overlap spatially, the SNR is improved by the square root of the overlap factor. In practice, nonuniformity of the detector array will introduce spatial noise that will affect MRTD; and even after

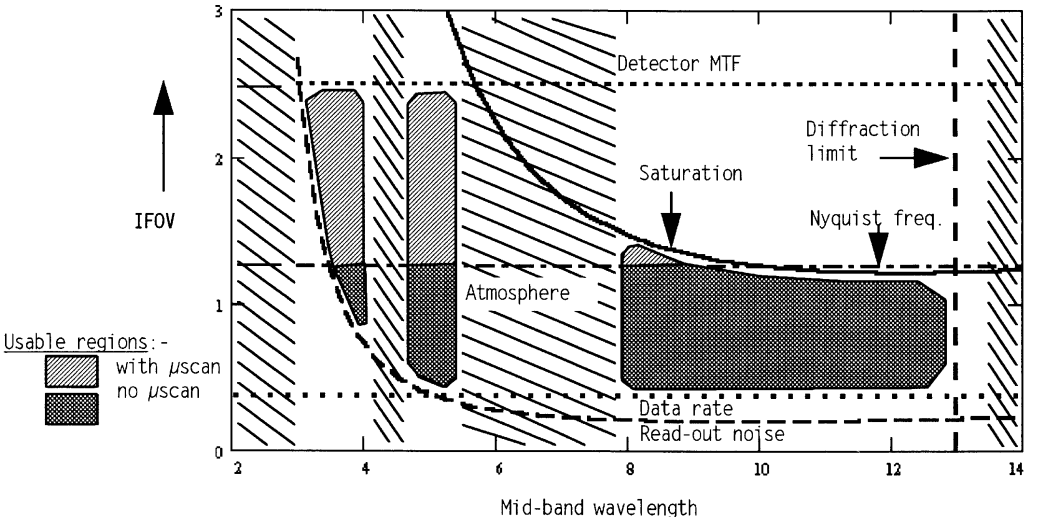

FIGURE 35.11 Physical limitations to thermal imaging when a specified spatial frequency must be resolved. The shaded regions indicate the combinations of wavelength and IFOV for which the task can be achieved. All the lines on the graph depend on system parameters such as aperture, quantum efficiency, read-out noise, and electron storage, but can be calculated from the equations given in the text.

electronic correction, this is frequently the main limitation on performance. Nonuniformity effects are discussed in [10] and [11].

The resulting trade-offs are discussed at some length in [12]. It is observed that if the integration time is controlled to prevent saturation, NETD is independent of *f*/number and quantum efficiency, but depends strongly on image contrast. This tends to favor the MWIR band, and makes high cold-shield efficiency crucial. The problem can be overcome in the LWIR by operating at a high frame rate, which has no effect on NETD but improves MRTD due to eye integration. For long-range applications, it is frequently necessary to use long focal lengths, giving large *f*/numbers if the optics diameter is to be kept within reasonable bounds. Under these conditions, saturation is less likely, and the high photon flux in the LWIR is necessary to overwhelm the read-out noise. If high spatial resolution rather than sensitivity is required, the MWIR band has a much better diffraction limit. Figure 35.11 indicates the ways in which the various limitations combine to define the combination of IFOV and waveband that gives optimum performance when it is necessary to resolve a given spatial frequency; the positions of the lines on this chart are of course peculiar to the system under investigation.

35.12 Future Trends in Thermal Imaging

At the high-performance end of the market, the developments are most likely to be driven initially by military requirements. Many countries already have thermal imaging common module programs, and many developments will be aimed at productionizing these modules to reduce cost and enhance performance. Multispectral instruments to aid in camouflage penetration and to broaden the conditions of operability through the atmosphere can be taken out of the laboratory into service. Currently, these are mainly scanning devices using adjacent long linear arrays of LWIR and MWIR detectors. For spectral agility, detector arrays based on multiquantum-well (MQW) technology can be used, since they can be tuned to some extent by varying the electrical bias. Multispectral refracting optics are complex and have poor transmission, so reflecting optics are generally used. Multispectral systems will allow more accurate compensation for emissivity, but their high cost might limit their use except for high-value applications such as earth resources surveys in aircraft or satellites. Techniques employed include frame-sequential filtering and imaging Fourier transform spectroscopy.

TABLE 35.2 Companies That Make Commercial Thermal Imagers

AGEMA Infrared Systems Inc.
550 County Avenue
Secaucus, NJ 07094
Tel: (201) 867-5390

Amber Engineering Inc.
57566 Thornwood Drive
Goleta, CA 93117-3802
Tel: (800) 232-6237, Fax: (805) 964-2185

Cincinnati Electronics Corporation
Detector and Microcircuit Devices Laboratories
7500 Innovation Way
Mason, OH 45040-9699
Tel: (513) 573-6275, Fax: (513) 573-6290

Hamamatsu Photonic Systems
360 Foothill Rd.
Bridgewater, NJ 08807-0910
Tel: (908) 231-1116, Fax: (908) 231-0852

Inframetrics Imaging Radiometer Group
12 Oak Park Drive
Bedford, MA 01730
Tel: (617) 275-8990, TWX: (710) 326-0659

Mitsubishi Electronics America Inc.
5665 Plaza Drive, P.O. Box 6007
Cypress, CA 90630-0007
Tel: (800) 843-2515

Nikos Corporation (Nikon)
1502 West Campo Bello Drive
Phoenix, AZ 85023
Tel: (602) 863-6182

Pilkington Optronics Inc
7550 Chapman Ave.
Garden Grove, CA 92841
Tel: (714) 373-6061, Fax: (714) 373-6074

Quest Integrated Inc.
21414-68th Avenue South
Kent, WA 98032
Tel: (206) 872-9500, Fax: (206) 872-8967

For commercial thermal imaging, the main thrust is likely to be cost reduction via the use of uncooled imagers, and in packaging to provide increased ease of use and functionality using in-built software. Optics cost can be reduced or performance improved by the use of hybrid aspheric components, which are now practical due to improvements in diamond turning. A diffractive surface is generated on one surface of a refracting lens. Because the power of a diffractive component is proportional to wavelength, a very low diffractive power can compensate for the chromatic aberration of the lens. This allows the use of materials such as zinc sulfide, which would otherwise be unacceptable due to chromatic aberration, but which have other desirable properties such as low cost or a low thermal coefficient of refractive index.

References

1. J.M. Lloyd, *Thermal Imaging Systems*, New York, Plenum Press, 1975, 20-21.
2. J.S. Acetta and D.L. Shumaker (eds.), *The Infrared & Electro-Optical Systems Handbook*, Bellingham, WA: SPIE Optical Engineering Press, 1993, Vol. 1, 52, 251-254.
3. F.X. Kneizys, E.P. Shettle, L.W. Abreu, G.P. Anderson, J.H. Chetwynd, W.O. Gallery, J.E.A. Selby, and S.A. Clough, *Users' Guide to LOWTRAN 7*, Report no. AFGL-TR-88-0177 Hanscom, Air Force Geophysics Laboratory, 1988.
4. M. Bass (ed.), *Handbook of Optics*, New York, McGraw-Hill, 1995, Vol. 1, chap. 23.
5. C.M. Hanson, Uncooled ferroelectric thermal imaging, in *Proc. SPIE 2020, Infrared Technology XIX*, 1993.
6. R.A. Wood, Uncooled thermal imaging with monolithic silicon focal plane arrays, *Proc. SPIE 2020, Infrared Technology XIX*, 1993, 329.
7. G.C. Holst, *Testing and Evaluation of Infrared Imaging Systems*, Winter Park, FL, JCD Publishing, 1993, 36-42.
8. M.J. Riedl, *Optical Design Fundamentals for Infrared Systems*, Bellingham, WA, SPIE Optical Engineering Press, 1995, 55.

9. L. Scott and J. D'Agostino, NVEOD FLIR92 thermal imaging systems performance model, *Proc. SPIE, Vol. 1689, Infrared Imaging*, 1992, 194-203.
10. A.F. Milton, F.R. Barone, and M.R. Kruer, Influence of nonuniformity on infrared focal plane performance, *Opt. Eng.*, 24, 855-862, 1985.
11. H.M. Runciman, Impact of FLIR parameters on waveband selection, *Infrared Phys. Technol.*, 37, 581-593, 1996.

Further Information

G. Gaussorgues, *Infrared Thermography*, London, Chapman and Hall, 1994.
F. Grum and R.J. Becherer (eds.), *Optical Radiation Measurements*, New York, Academic Press, 1979, Vol. 1.
G.C. Holst, *Electro-optical Imaging System Performance*, Winter Park, FL, JCD Publishing, 1993, 36-42.
C.L. Wyatt, *Radiometric Calibration: Theory and Methods*, New York, Academic Press, 1978.